# HEIGHT PRESSURE EFFECT ON STRUCTURAL, ELASTIC VIBRATIONAL AND THERMODYNAMIC PROPERTIES OF CHALCOPYRITE CDGEP$_2$ FROM FIRST PRINCIPLES CALCULATIONS

**Guenfoud, Mohammed**
LDDI–Laboratory, Faculty of Science and Technology, University Ahmed Draia of Adrar,01000,Algeria
moh.guenfoud@univ-adrar.edu.dz

**Hamouda Messaoud**
LDDI–Laboratory, Faculty of Science and Technology, University Ahmed Draia of Adrar,01000,Algeria
mes.hamouda@univ-adrar.edu.dz

## ABSTRACT

The structural, vibrational, elastic and thermodynamic properties of the chalcopyrite structure CdGeP$_2$ under pressure have been investigated by first principles calculations in the frame of the density functional theory (DFT). The obtained lattice parameter and bulk modulus under zero pressure and zero temperature are in excellent agreement with the available experimental data and other theoretical results. The phonon dispersion spectra and the obtained elastic constants shows that the CdGeP$_2$ compound is mechanically and dynamically stable up to 10 GPa and no evidence of any phase transition. The pressure dependences of the elastic constants $C_{ij}$, bulk modulus $B$, shear modulus $G$, Young's modulus $E$, Poisson ratio $\nu$ and compressibility $K$ of CdGeP$_2$ are also successfully obtained and discussed. In addition, the thermodynamic properties of CdGeP$_2$ , such as Helmholtz free energy $F$, internal energy $E$, entropy $S$ and The heat capacity $C_V$ are predicted by the quasi-harmonic approximation.

**Keywords:** Elastic properties; vibrational properties; Thermodynamic properties; high pressure; quasi-harmonic approximation.

## 1. INTRODUCTION

The ternary compounds II–IV–V2 chalcopyrite materials have attracted considerable scientific attention in recent years due to their promising applications in the fields of optoelectronics, photovoltaic and non-linear optic (NLO) [1-3]. One of this group of materials, CdGeP$_2$, is widely used in solar cells, optical parametric oscillators, infrared light emitting diodes and detectors [4, 5]. Moreover, its proper direct band gap (1.44 eV), large absorption coefficient ($>10^5$ cm$^{-1}$), and low cost add to the advantages for photovoltaic application [6, 7]. Very recently, Zhang et al. [8] have been successfully grown the single crystals with the dimension of 40 mm in length and 8 mm in diameter using vertical Bridgman technique. Nowadays, very few studies have been performed [9-13]. On the theoretical side, the elastic properties of CdGeP$_2$ under pressure have been investigated for the first time by Gautam et al. by using FP-LAPW method [14, 15] as implemented in the WIEN2K code [16]. Elastic constants are very important quantities to describe the mechanical properties of materials. Values of elastic constants provide valuable information on the structural stability and the anisotropic. Therefore, systematic investigation on elastic, thermodynamic and dynamical properties of CdGeP$_2$ at different pressure could be used to predict the basic parameters of material.

In this paper, we have used the density functional theory to calculate the structural, elastic, dynamical, and thermodynamic properties of CdGeP$_2$ under different hydrostatic pressure. The dynamic

stability was verified by analyzing the corresponding phonon spectrum under various pressures. The thermodynamic properties were obtained by using a quasi-harmonic approximation method. The obtained values of all parameters are in good agreement with the available theoretical values. This paper is organized as follows: the theoretical method is introduced and the computation details are given in section 2. In section 3, the results are presented and discussed. Finally, a summary of our main results is given in Sect. 4.

## 2. COMPUTATIONAL DETAILS

The structural optimization and vibrational properties are conducted using the Vienna Ab-initio Simulation Package (VASP) code [17–21] within the framework of the density-functional theory (DFT) [22]. In this work, all calculations were performed within the generalized gradient approximation (GGA) with the exchange-correlation functional proposed by Perdew-Burke-Ernzernhof prescription for solids (GGA-PBEsol) [23]. The valence electronic configurations for Cd, Ge, and P were $4d^{10} 5s^2$, $3d^4 s^4 p$ and $3s^2 2p^3$, respectively.

The plane-wave basis set of cutoff energy was set to 560 eV, and the Brillouin zone was sampled over
$8 \times 8 \times 8$ points by the Monkhorst–Pack scheme [24]. The total energy was calculated with high precision, converged to $10^{-8}$ eV/atom, and the atomic relaxation was stopped when the ionic Hellmann-Feynaman forces become less than $10^{-3}$ eV/Å.
The phonon calculations are performed by the linear response approach as implemented in the PHONOPY code [25], in combination with VASP.

The $2 \times 2 \times 2$ supercell (128 atoms) constructed from the conventional unit cell (16 atoms, six coordination shells) and a $2 \times 2 \times 2$ k-mesh were used to calculate the force constants, The vibrational properties including the phonon dispersion curves and phonon density of states, as well as the phonon frequencies at the Brillouin zone center are obtained in the framework of the density functional perturbation theory (DFPT) [26].

## 3. RESULTS AND DISCUSSIONS
### 3.1. Structural optimisation

CdGeP$_2$ ternary compounds usually crystallize in the body-centered-tetragonal chalcopyrite structure belonging to the I$\overline{4}$2d (No.122) space group, with the Cd, Ge, and P atoms occupying the Wyckoff sites of 4a, 4b, and 8d, represented in Fig.1. The chalcopyrite structure is deduced from that of the zinc-blende by the replacement of the cationic sublattice by two different atomic species. Generally, the chalcopyrite structure is characterized by three structural parameters: the lattice constants a and c, as well as the dimensionless anion displacement parameter *u* defined by the following relation ship [27, 28]:

$$u = 0{,}25 + (d^2_{II–V} − d^2_{IV–V})/a^2 \qquad (1)$$

where $d_{II–V}$ and $d_{IV–V}$ are the bond lengths between the atoms of the corresponding groups. In an ideal chalcopyrite structure, the equalities $\gamma = c/a = 2.0$ and $u = 0{,}25$ holds true.
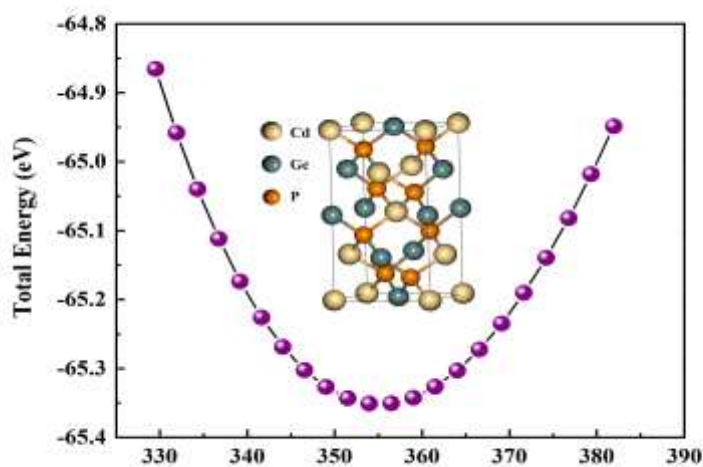
**Fig. 1** The total energy per formula unit as function of volume for CdGeP$_2$. The inset is the corresponding crystal structure.

The ground state structural properties are obtained by minimization of the total energy with respect to the unit cell volume around the equilibrium cell volume $V_0$. The calculated (E-V) data are fitted to the Birch- Murnaghan EOS [29]. Fig.1 shows the total energy as a function of the conventional-cell volume for CdGeP$_2$, and the inset shows the crystal structure of CdGeP$_2$. The calculated lattice constants $a$ $(c)$, axial ratio $c/a$, internal parameter $u$, bulk modulus $B$ and volume $V$ are presented in table 1, together with the available experimental and theoretical results.

**Table 1.** The equilibrium lattice constant $a$ $(c)$ (in unit Å), axial ratio $c/a$, cell volume $V$(Å$^3$) ,internal parameter $u$  and bulk modulus $B$ (GPa)  for CdGeP$_2$ .

| Method | $a$ | $c$ | $c/a$ | $V$ | $u$ | $B$ |
|---|---|---|---|---|---|---|
| Present work (VASP-GGA-PBEsol) | 5.722 | 10.843 | 1.895 | 355.01 | 0.277 | 73.15 |
| WIEN2K-WC-GGA (Ref. [30]) | 5.680 | 11.110 | 1.956 | 358.44 | 0.262 | - |
| VASP-GGA (Ref. [31]) | 5.815 | 11.007 | 1.893 | 372.23 | 0.278 | 72.0 |
| VASP-GGA (Ref. [32]) | 5 .811 | 10 .976 | 1.889 | 370.64 | 0 .283 | 65.2 |
| Exp. (Ref. [33]) | 5.740 | 10.776 | 1.877 | 355.04 | 0.282 | - |
| Exp. (Ref. [34]) | 5.738 | 10.765 | 1.876 | 354.43 | 0.282 | - |

From the table, in our GGA-PBEsol calculations, the predicted lattice constants of CdGeP$_2$ are a = 5.722 Å and c = 10.843 Å, which are very close to the experimental works [33]. Figure 2b shows the dependence of the lattice constants on the pressure up to 10 GPa. It can be seen that the obtained lattice constants gradually decrease with the pressure increase. The variation of the lattice constants (a and c) presents anisotropic property when external pressure is applied. To display the anisotropic character more clearly, the reduced lattice constants are plotted in Figure 1a, where $a_0$ and $c_0$ are the lattice constants at 0 pressure. We can observe that the $(c/c_0)$ drops faster than the $(a/a_0)$ with pressure, which demonstrates that chalcopyrite-type compound CdGeP$_2$ is easily compressed along the c direction.
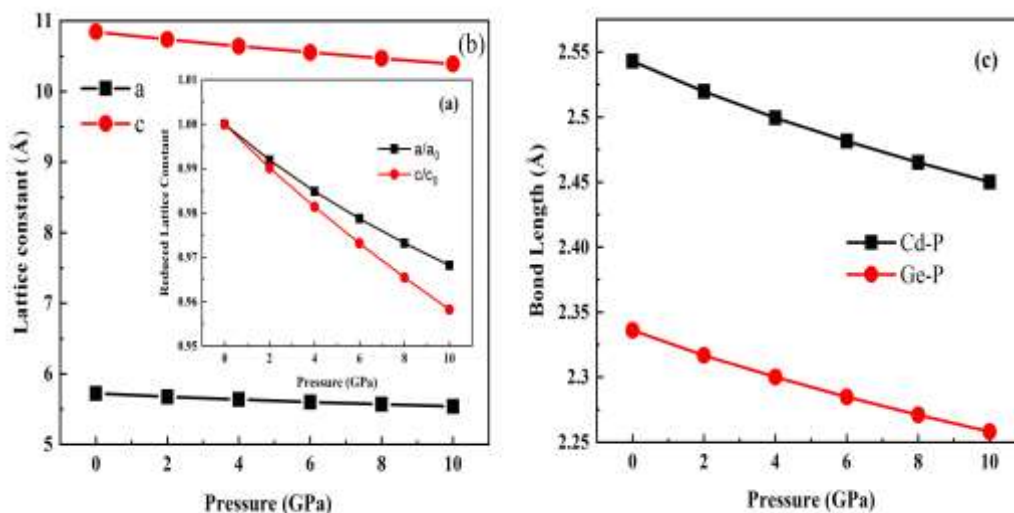
**Fig. 2** (**a**) Reduced  lattice constants, (**b**) calculated lattice constants, and  (c) bond lengths of Cd-P and Ge-P for the chalcopyrite-type $CdGeP_2$ as a function of the  hydrostatic pressure.

The bond length is one of the important structural parameters. To further clarify the effect of the pressure on the structure, the hydrostatic pressure dependence on the bond length is shown in Figure 2c. It can be seen that the bond lengths of Cd-P and Ge-P for chalcopyrite type compound $CdGeP_2$ under 0 pressure are 2.543 Å, 2.336 Å, respectively. It is worth noting that the bond lengths of Cd-P and Ge-P for chalcopyrite-type compound $CdGeP_2$ decrease gradually with the increasing hydrostatic pressure in the range of the pressure studied. Moreover, the bond length of Cd-P is more sensitive than that of Ge-P with the increasing hydrostatic pressure.

## 3.2 Elastic Properties

The elastic constants are among the most fundamental parameters of materials that can be predicted from the first-principles ground-state total-energy calculations. Most importantly, these constants can provide valuable informations about the nature of the forces exerting on solids as well as the phase stability and stiffness of materials. It is known that The elastic stiffness tensor of chalcopyrite compounds has six independent components because of the symmetry properties of the $I\bar{4}2d$  space group, namely $C_{11}$, $C_{12}$, $C_{13}$, $C_{33}$, $C_{44}$ and $C_{66}$ in Young's notation, respectively. Unfortunately, to our knowledge, there are no experimental values about the elastic constants have been reported for $CdGeP_2$, therefore, to check the reliability of our calculated values, we checked firstly the obtained constants according to Born elastic stability criteria [35], which for the tetragonal  crystals are :

$$C_{11} > |C_{12}| \tag{2}$$
$$2C^2_{13} < C_{33} (C_{11} + C_{12}) \tag{3}$$
$$C_{11} > 0 , C_{33} > 0 , C_{44} > 0 , C_{66} > 0 \tag{4}$$

The calculated elastic constants, with an analogous set of six independent compliances $S_{ij}$ are given in Table 2. It can be seen clearly that our calculated elastic constants satisfy all these conditions, implying that $CdGeP_2$ crystal is mechanically stable. From the calculated elastic constants, the bulk modulus *B can* be computed by the Voigt approach (uniform strain assumption) [36]

$$B_V = \frac{1}{9}(2C_{11} + C_{33} + 2C_{12} + 4C_{13}) \tag{5}$$

And from the Reuss approach [37] by

$$B_R = \frac{(C_{11} + C_{12})C_{33} - 2C_{13}^2}{C_{11} + C_{12} + 2C_{33} - 4C_{13}} \tag{6}$$

Therefore, shear modulus upper bounded by can be presented as [36]

$$G_V = \frac{1}{15}(2C_{11} + C_{33} - C_{12} - 2C_{13} + 6C_{44} + 3C_{66}) \tag{7}$$

And lower bounded by [37]

$$G_R = 15\left\{\frac{18B_V}{C^2} + \frac{6}{(C_{11} - C_{12})} + \frac{6}{C_{44}} + \frac{3}{C_{66}}\right\}^{-1} \tag{8}$$

where $C^2 = (C_{11} + C_{12})C_{33} - 2C_{13}^2$

From the Voigt–Reuss–Hill approximations [38], the arithmetic average of Voigt and Reuss bounds is written as

$$B = \frac{1}{2}(B_V + B_R) \tag{9}$$

$$G = \frac{1}{2}(G_V + G_R) \tag{10}$$

The Young's modulus $E$ and Poisson's ratio are obtained as

$$E = \frac{9BG}{3B + G} \tag{11}$$

$$\nu = \frac{3B - 2G}{2(3B + G)} \tag{12}$$

Finally the linear compressibilities $\kappa_a$ and $\kappa_c$ along the $a$- and $c$- axis respectively for the tetragonal structure are given in term of elastic constants by the following relations

$$\kappa_a = -\frac{1}{a}\frac{\partial a}{\partial p} = \frac{C_{33} - C_{13}}{C_{33}(C_{11} + C_{12}) - 2C_{13}^2} \tag{13}$$

$$\kappa_c = -\frac{1}{a}\frac{\partial c}{\partial p} = \frac{C_{11} + C_{12} - 2C_{13}}{C_{33}(C_{11} + C_{12}) - 2C_{13}^2} \tag{14}$$

All materials are anisotropic, hence, the orientation-dependent properties are very important to study, predict and design new materials with optimal properties for various applications. With the knowledge of elastic stiffness constants presented above it is possible to calculate the direction dependent Young's modulus ($E$) and the direction dependent linear compressibility ($\beta$). Their formulas for tetragonal crystals are [39]

$$\frac{1}{E} = S_{11}\left(l_1^4 + l_2^4\right) + \left(2S_{13} + S_{44}\right)\left(l_1^2 l_3^2 + l_2^2 l_3^2\right) + S_{33}l_3^4 + \left(2S_{12} + S_{66}\right)l_1^2 l_2^2 \tag{15}$$

$$\beta = \left(S_{11} + S_{12} + S_{13}\right) - \left(S_{11} + S_{12} - S_{13} - S_{33}\right)l_3^2 \tag{16}$$

where $(l_1, l_2, l_3)$ are are the direction cosines in the sphere coordination, $S_{ij}$ are the elements in the tensor of CdGeP$_2$, which is the inverse of the elastic tensor.

In Tables 2 and 3, we present our calculated properties. Such as elastic constants ($C_{11}$, $C_{12}$, $C_{13}$, $C_{33}$, $C_{44}$ and $C_{66}$) and bulk modulus $B$ (GPa), shear modulus $G$ (GPa), Young modulus $E$ (GPa), Poisson's ratio $v$ and the linear compressibilities $\kappa_a$ (GPa$^{-1}$), $\kappa_c$ (GPa$^{-1}$) along the   $a$- and $c$- axis

respectively of CdGeP$_2$ under pressure 0 GPa. We can see that $C_{11}$ has bigger value than $C_{33}$ which means that CdGeP$_2$ is easily compressed along the c-axis than a-axis.

**Table 2** Elastic constants $C_{ij}$ (in GPa) of CdGeP$_2$ under pressure 0 GPa.

| Refs. | $C_{11}$ | $C_{12}$ | $C_{13}$ | $C_{33}$ | $C_{44}$ | $C_{66}$ |
|---|---|---|---|---|---|---|
| This work | 109 | 57 | 59 | 96 | 47 | 46 |
| Ref. [30] | 107 | 61 | 63 | 102 | 47 | 48 |
| Ref. [31] | 102.1 | 46.7 | 50.2 | 89.3 | 66.0 | 69.1 |
| Ref. [40] | 84 | 53 | 50 | 79 | 29 | 26 |

From the table 2, in our GGA-PBEsol calculations, we can see that the calculated values are excellently in agreement with other theoretical works [30, 31]. Similarly to the elastic constant tensor, the bulk $B$ and the shear moduli $G$ provide information regarding the material hardness under deformation. These properties can be directly computed from the elastic constants tensors [36].

**Table 3** Calculated  bulk modulus $B$ (GPa), shear modulus $G$ (GPa), Young modulus $E$ (GPa), Poisson's ratio $v$ and the linear compressibilities $\kappa_a$ (GPa$^{-1}$), $\kappa_c$ (GPa$^{-1}$) along the $a$- and $c$- axis respectively of CdGeP$_2$ under pressure 0 GPa.

| Refs. | $B$ | $G$ | $E$ | $v$ | $\kappa_a$ | $\kappa_c$ |
|---|---|---|---|---|---|---|
| This work | 73.48 | 35.26 | 91.19 | 0.293 | 0.0043 | 0.0051 |
| Ref. [30] | 76.63 | 34.43 | 89.84 | 0.300 | 0.0043 | 0.0045 |

The calculated bulk modulus B of the CdGeP$_2$ at 0 K and 0 GPa is 73.48 GPa, which is in agreement with the result of 73.15 GPa obtained from fitting Birch-Murnaghan EOS.

The calculated pressure dependences of the elastic constants at 0 K are also plotted in Fig.3. Through careful observation in Fig. 3, we can note that $C_{11}$, $C_{12}$, $C_{13}$, and $C_{33}$ are sensitive to pressure, especially for $C_{11}$ and $C_{33}$ vary notably with the applied pressure, while $C_{44}$ and $C_{66}$ vary slightly with the applied pressure. Moreover, the $C_{11}$ is more sensitive to pressure than $C_{12}$ and $C_{44}$. This is due to the fact that $C_{11}$ represents elasticity in length, $C_{12}$ and $C_{44}$ are related to the elasticity in shape; a longitudinal strain produces a change in C11, while a transverse strain causes a change in shape not in volume.
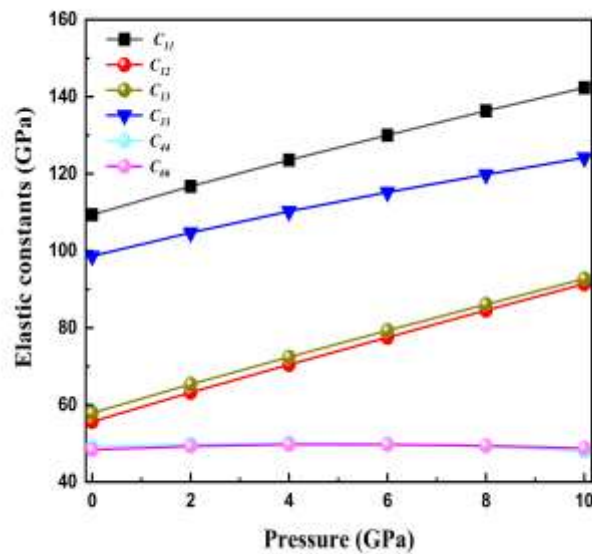
**Fig. 3** Pressure dependence of elastic constants of CdGeP$_2$ at 0 K.

The high/low value of the G/B ratio is associated with ductility/brittleness. The critical value separating the ductile and brittle materials is conventionally set to 0.5 . The G/B values calculated for the compound under examination are lower than 0.5, implying ductile behaviour.
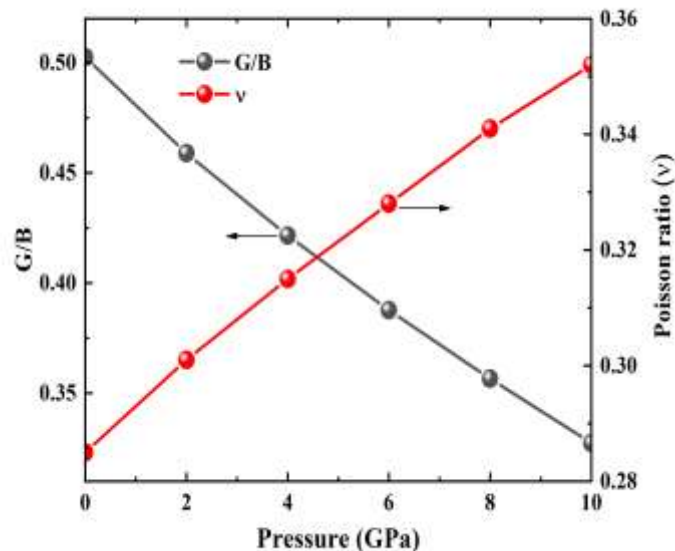


**Fig. 4** Pressure dependence of G/B ratio and Poisson's ratio $v$ of CdGeP$_2$ at 0 K.

From our high-pressure elastic constants, we calculated the bulk modulus B, shear modulus G, and Young's modulus E from the Voigt-Reuss-Hill approximations [38].

As shown in Fig. 5, the calculated bulk modulus B increase monotonously with increasing pressure, so it indicates that CdGeP$_2$ is becoming more and more difficult to be compressed with the increasing pressure, while the variation of shear modulus G and Young's modulus E mains almost invariant with increasing pressure.
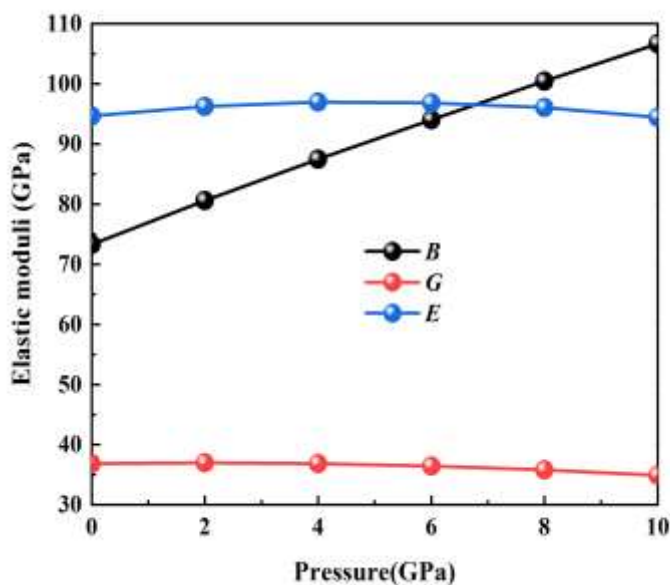
**Fig. 5** Pressure dependence elastic moduli of CdGeP$_2$ at 0 K.

To better understand the anisotropic behaviour, we obtained the 3D surface representations of the direction-dependent Young's modulus and its plane projections at 0 and 10 GPa, as shown in figure 6(a–d). From figure 6, we can see that the (001) plane exhibits isotropic property but the (100) and (010) planes exhibit anisotropic behaviour at 0 GPa; these results are consistent with those obtained by Hou et al. [31]

In addition, for an isotropic system, the curved surface should be spherical, while the deviation from the spherical shape indicates the extent of elastic anisotropy. From figure 6c,d, it is not difficult to find that the anisotropy is significant with increase in pressure. For CdGeP$_2$, at ground state, the obtained figure deviates a little from the spherical shape, which means that CdGeP$_2$ has a slightly elastic anisotropy, consistent with the previous discussion.

It is shown clearly that the Young's modulus show a high degree of anisotropy along different crystallographic orientations from 0 up to 10 GPa, and the anisotropy characteristic is becoming more and more significant with the increasing of applied pressure.

In order to denote the elastic anisotropy more visually, the linear compressibility in Fig. 7 is plotted. The 3D figure of the linear compressibility for the tetragonal CdGeP$_2$ is characterized by more anisotropic along the z axis than that along the x and y axis. From Fig. 7, It can see that the direction dependent linear compressibility in the (001) plane is isotropic, but that in the (100) plane is not. The values in the (001) plane are smaller than those in the (100) and (110) planes.
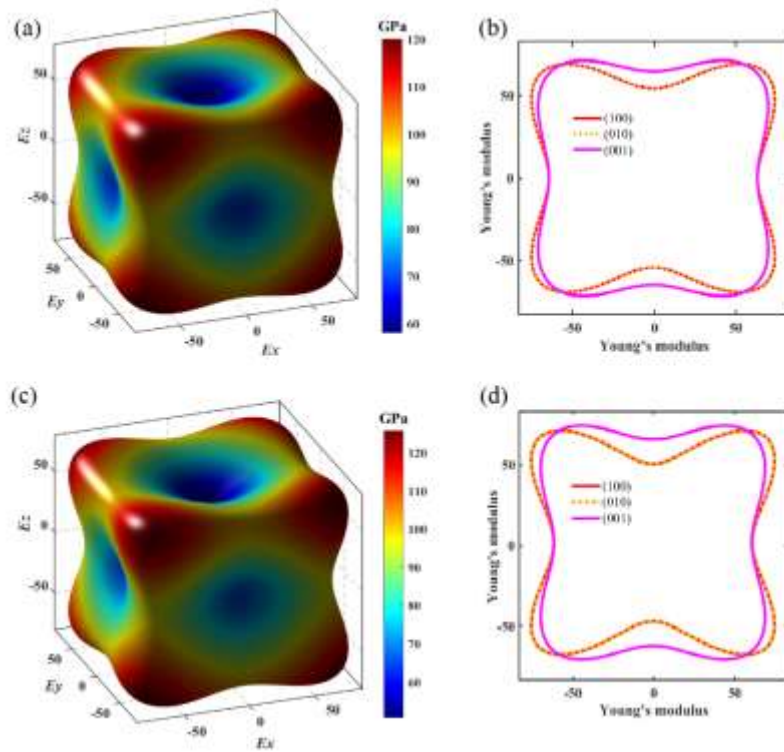
**Fig. 6** The directional dependence of Young's modulus (GPa) and its plane projections for CdGeP$_2$ at 0 (a,b) and 10 GPa (c,d).
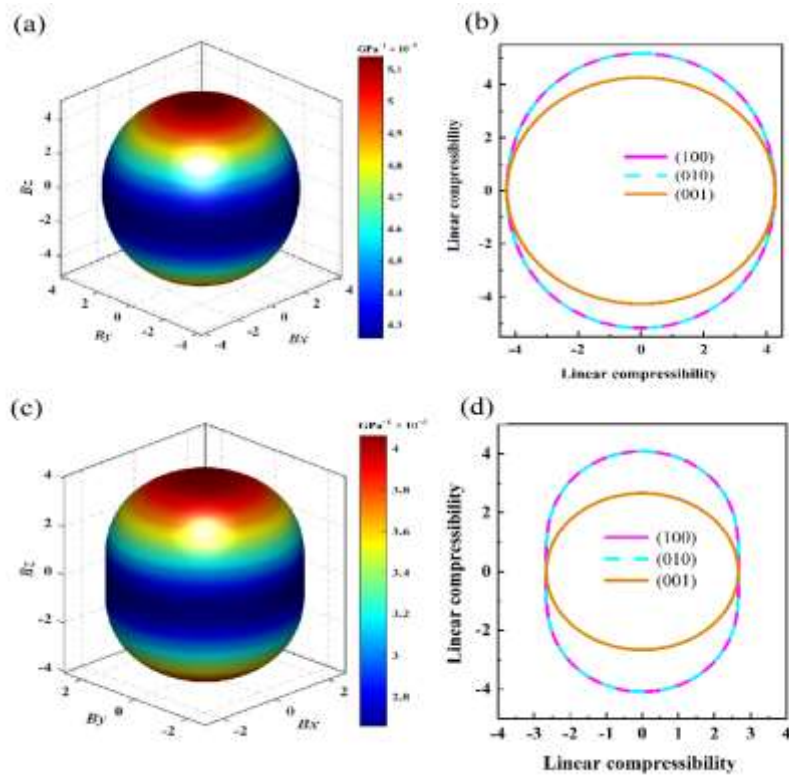


**Fig. 7** The directional dependence of linear compressibility (TPa$^{-1}$) and its plane projections for CdGeP$_2$ at 0 (a,b) and 10 GPa (c,d).

### 3.3. Vibrational Properties

Group theory analysis, for the space group I-42d shows that the irreducible representation of the acoustic and optical vibrational modes at center point $\Gamma$ can be represented as:

$$\Gamma_{aco} = B_2 + E \tag{17}$$

$$\Gamma_{opt} = A_1 + 2A_2 + 3B_1 + 3B_2 + 6E$$

Since the unit cell of chalcopyrite structure contains eight atoms, the vibrational spectrum involves Twenty-four branches: 3 acoustic branches and 21 optical branches. According to the selection rules of infra-red (IR) absorption and Raman scattering, among these 24 modes, all modes, except $A_2$ mode, are Raman active, and only $B_2$ and $E$ modes are IR active. Furthermore, the $A_2$ vibrational mode is called silent vibrational mode, since it is neither infrared nor Raman active. There are totally thirteen Raman-active (R) modes, nine IR-active (IR) modes and two silent (S) modes for $CdGeP_2$ compound.

The calculated phonon dispersion curve of $CdGeP_2$ compound along the high symmetry points in the first Brillouin zone and the corresponding phonon density of states (DOS) are shown in Fig.8.a and 9.c.

It can be seen clearly that there is no soft modes found at any wave vectors above in the phonon dispersion curve, implying that this structure is mechanically stable below 10 GPa.
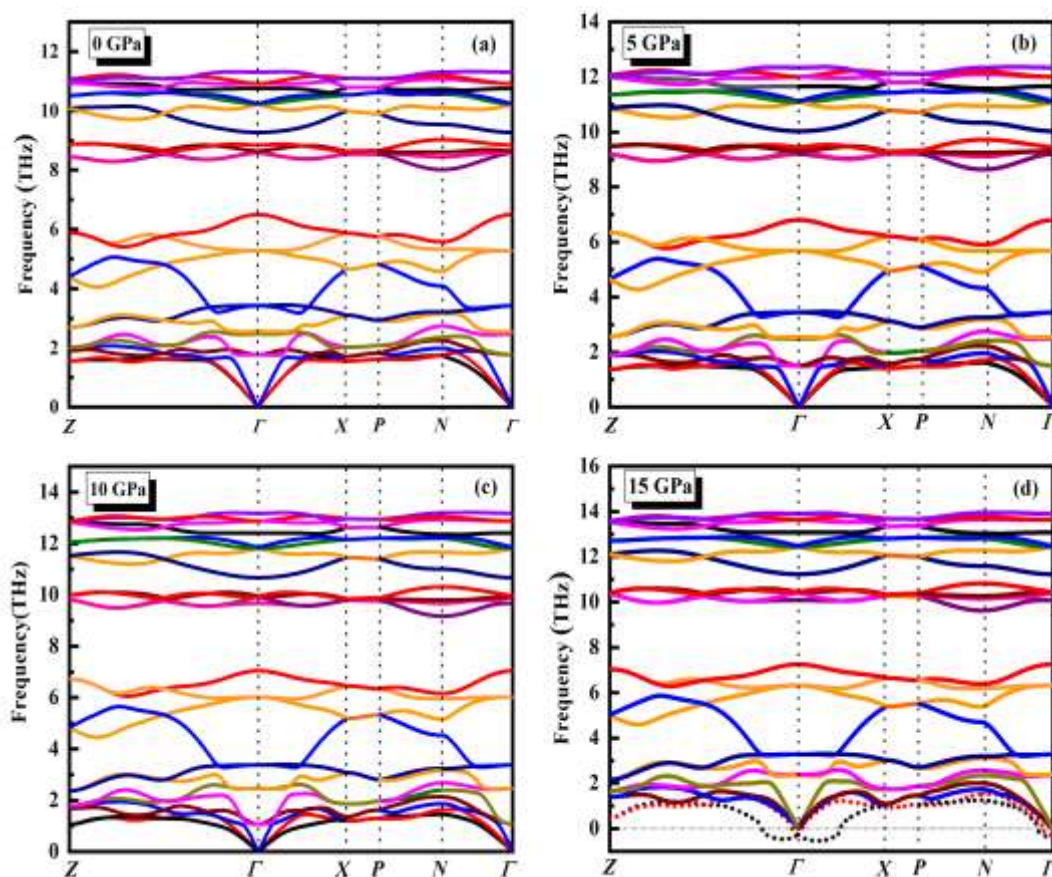


**Fig. 8** Phonon spectrums along the high-symmetry directions of $CdGeP_2$ at different hydrostatic pressures: (**a**) 0 GPa; (**b**) 5 GPa; (**c**) 10 Gpa; (**d**) 15 GPa.

The partial phonon DOS curve in Figure 9.a shows that the vibration of the Cd atom governs the acoustic branches. We can distinguish relatively three region s at point $\Gamma$: The low frequency zone around 0-4 THz, come overall from the vibration of Cd atoms owing to its heavy atomic weight, a medium frequency zone between 4 and 10 THz, results from the vibration of the three constituent atoms, especially the Ge and P atoms, a high frequency zone above 10 THz are mainly from the vibration of P atom with low contribution from atom Ge due to their light atomic weight compared to that of the Cd atom. This is consistent with the curve of the phonon dispersion.

The phonon dispersion curve calculations were performed up to 20 GPa with an interval of 2 GPa. A more careful calculation at 15 GPa was performed for determining the precise pressure value when the phonon became instable. The phonon dispersion curve in figure 9.d shows an obvious imaginary frequency near the center point $\Gamma$. The appearance of the imaginary frequency is a sure sign of a dynamic instability at the related pressure. Besides, the closeness between the frequencies of some optical and acoustic modes means that energy transfer between these modes is easy. It is interesting to note that as the pressure increases, most phonon modes shift to higher frequencies, while one optical phonon branch around the $\Gamma$ point decreases in frequency. Moreover, the frequency gap between two bands becomes wider. From Figure 9d we notice that the $CdGeP_2$ is dynamically instable at high pressure (above 15 GPa)
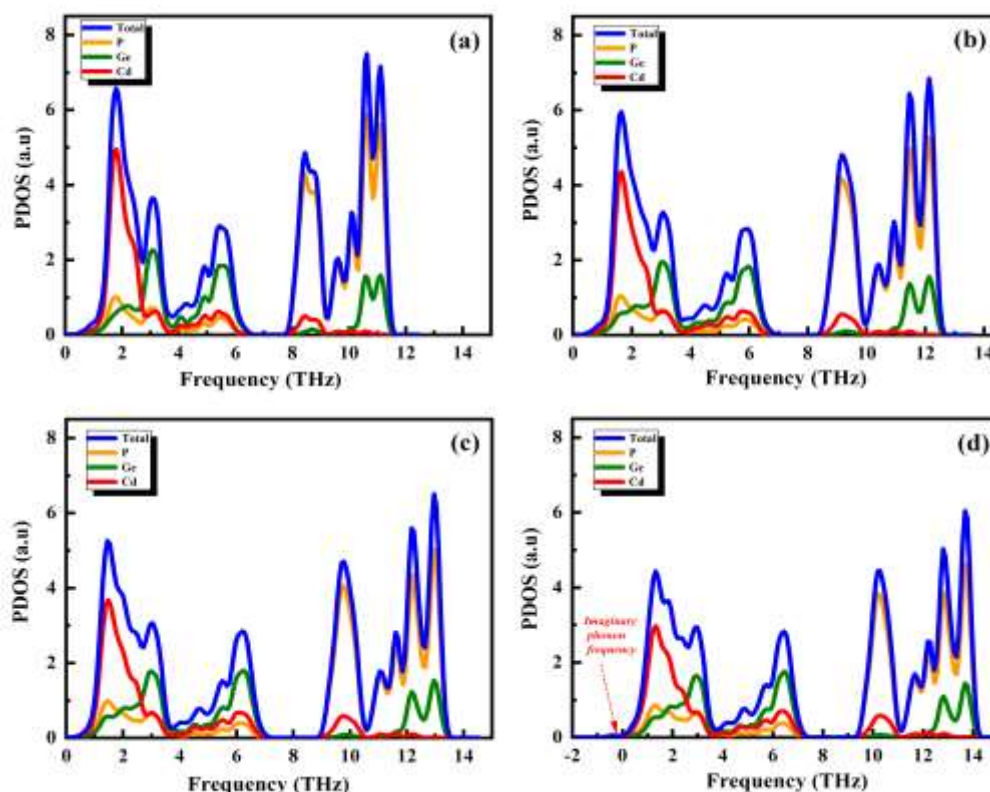


**Fig. 9** Phonon density of states of $CdGeP_2$ at different hydrostatic pressures: (**a**) 0 GPa; (**b**) 5 GPa; (**c**) 10 GPa; (**d**) 15 GPa.

Table 4 lists the optical vibrations modes and their corresponding frequencies of $CdGeP_2$ compound calculated at $\Gamma$ point in the Brillouin zone. Our calculated frequencies are very close to the theoretical data in Ref. [32].

**Table 4** Phonon frequencies (THz) at zone center ($\Gamma$ point) of CdGeP2

| Mode symmetry | Present | Ref. [32] | Ref. [31] | Ref. [41] | Ref. [41] |
|---|---|---|---|---|---|
| $E(R,I)$ | 1.77 | 1.77 | 1.66 | 1.84 | 1.89 |
| $E(R,I)$ | 3.42 | 3.45 | 3.40 | 3.46 | 3.63 |
| $E(R,I)$ | 5.30 | 5.33 | 5.41 | 5.68 | 5.36 |
| $E(R,I)$ | 8.58 | 8.65 | 8.72 | 8.60 | 8.66 |
| $E(R,I)$ | 10.24 | 10.32 | 10.58 | 10.62 | 10.61 |
| $E(R,I)$ | 10.92 | 11.03 | 11.40 | 11.46 | 11.54 |
| $B_1(R)$ | 2.47 | 2.49 | 2.45 | 2.56 | 2.55 |
| $B_1(R)$ | 6.50 | 6.52 | 6.60 | 6.61 | 6.74 |
| $B_1(R)$ | 10.76 | 10.83 | 11.07 | 11.15 | 11.18 |
| $B_2(R,I)$ | 2.55 | 2.58 | 2.51 | 2.71 | 2.64 |
| $B_2(R,I)$ | 8.64 | 8.67 | 8.73 | 8.79 | 8.84 |
| $B_2(R,I)$ | 11.30 | 11.38 | 11.73 | 11.63 | 11.60 |
| $A_2$ | 8.84 | 8.89 | 8.94 | 8.90 | - |
| $A_2$ | 10.21 | 10.30 | 10.57 | 10.44 | - |
| $A_1(R)$ | 9.27 | 9.32 | 9.50 | 9.67 | 9.62 |

## 3.4. Thermodynamic properties

From the phonons dispersion curve and phonon densities of states, The Thermal properties such as the phonon contribution to the internal energy $\Delta E$, the phonon contribution to the Helmholtz free energy $\Delta F$, as well as the entropy $S$ and the constant-volume specific heat $C_V$, at temperature $T$ are obtained immediately with the known expressions [42]:

$$\Delta F = 3nNk_BT \int_0^{\omega_L} In\left\{2\sinh\frac{\hbar\omega}{2k_BT}\right\}g(\omega)d\omega$$

$$\Delta E = 3nN\frac{\hbar}{2}\int_0^{\omega_L}\omega\coth\left(\frac{\hbar\omega}{2k_BT}\right)g(\omega)d\omega$$

$$C_V = 3nNk_B\int_0^{\omega_L}\left(\frac{\hbar\omega}{2k_BT}\right)^2\csc h^2\left(\frac{\hbar\omega}{2k_BT}\right)g(\omega)d\omega \tag{19}$$

wh
$\omega$ is t$\Bigg|$ $S = 3nNk_BT\int_0^{\omega_L}\left[\frac{\hbar\omega}{2k_BT}\coth\frac{\hbar\omega}{2k_BT} - In\left\{2\sinh\frac{\hbar\omega}{2k_BT}\right\}\right]g(\omega)d\omega$ states .     ll,

The phonon contribution to the internal energy $\Delta E$ and the phonon contribution to the Helmholtz free energy $\Delta F$ are presented in Fig.10. It can be seen clearly that as temperature increases from 0 K up to 1000 K, the relative internal energy ($\Delta E$) increases gradually, while the relative Helmholtz free energy ($\Delta F$) decreases gradually at various pressures for CdGeP2.
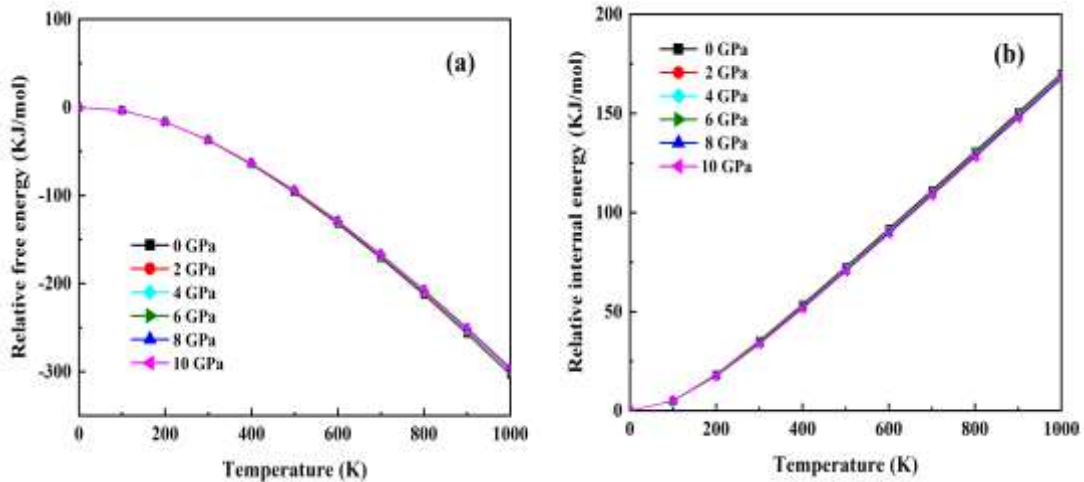
**Fig.10** Relative Helmholtz free energy $\Delta F$ (a) and relative internal energy $\Delta E$ (b) at various pressures for CdGeP$_2$.

Figure 11 shows that as the temperature increases, the entropy increases smoothly. Unfortunately, there are no experimental data available related to the entropy of CdGeP$_2$ in the literature for comparison.
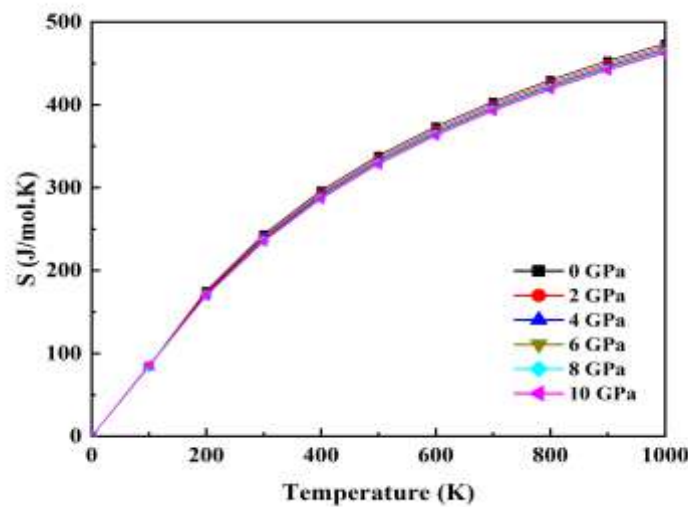


**Fig.11** Entropy vs temperature at various pressures for CdGeP$_2$.

The calculated heat capacity C$_V$ of CdGeP$_2$, as a function of T at various pressures is shown in Fig.12. It is shown that at the room temperature of 300 K, the value of $C_V$ is 178,30 J/ mol.K. At high temperature the heat capacity C$_V$ approaches classical asymptotic the Dulong–Petit limit.
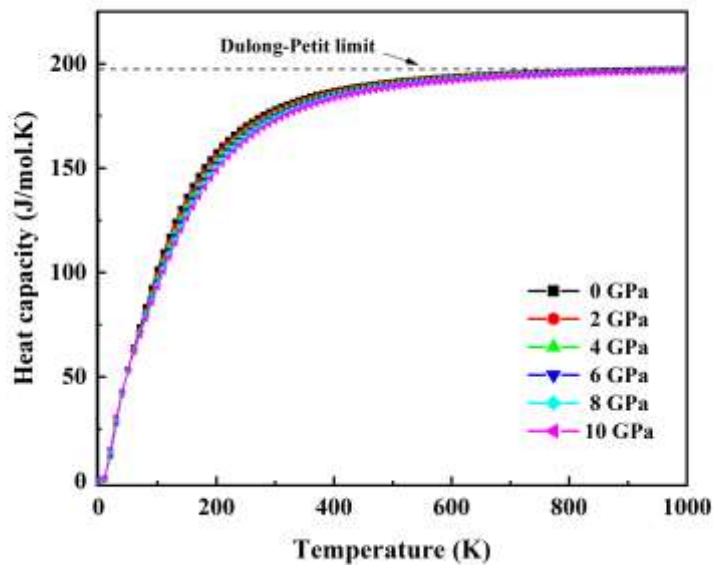
**Fig.12**. The constant-volume heat capacity $C_V$ at various pressures for CdGeP$_2$.

Our calculation of the heat capacities C$_P$ and C$_V$ of CdGeP$_2$ as a function of T are shown in the figure 13. From these figure, it can be seen that the constant volume heat capacity C$_V$ and the constant pressure capacity C$_P$ are very similar in appearance and both of them are proportional to T$^3$ at low temperatures. At high temperatures, the anharmonic effect on heat capacity is suppressed; which is called Dulong-Petit limit, with the increase of the temperature, whereas C$_P$ increases monotonically with the temperature.
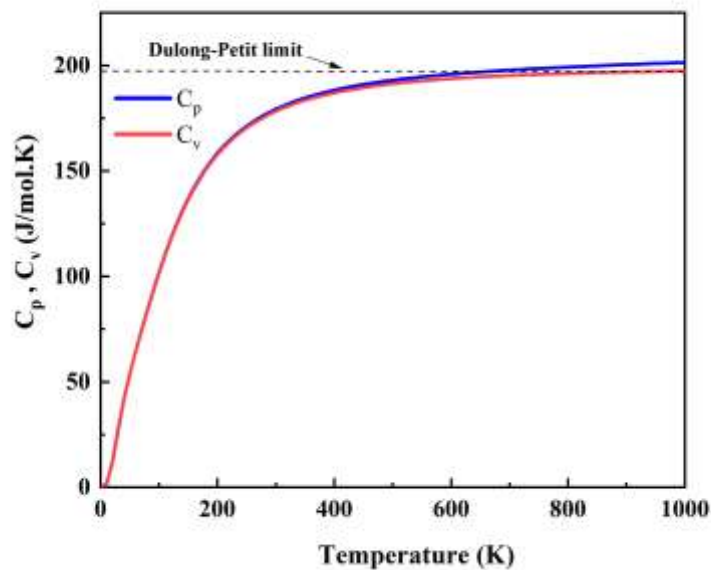


**Fig.13**. Heat capacity of constant volume $C_V$ and constant pressure Cp as a function of temperature at 0 GPa

## 4. CONCLUSIONS

Our first-principles study was focused on the structural, elastic, dynamical, and thermodynamic properties of $CdGeP_2$ under pressures. The results showed the pressure has the significant impact on the lattice parameters and elastic, dynamical, and thermodynamic properties of $CdGeP_2$. The obtained lattice parameter and bulk modulus under zero pressure and zero temperature are in excellent agreement with the available experimental data and other theoretical results. The dynamical properties of $CdGeP_2$ have been determined using the linear response approach to density functional perturbation theory (DFPT) successfully. The calculated elastic constants showed that this compound is mechanically stable. In the calculated phonon dispersion curves, there are no soft modes at any wave vectors, which confirm the dynamical stability of $CdGeP_2$ under zero pressure and zero temperature. The Helmholtz free energy, the internal energy, the entropy, the Heat capacity of constant volume and constant pressure has also been obtained by using the quasi-harmonic approximation QHA. Finally, we have found that the $CdGeP_2$ compound is dynamically instable at high pressure (above 15 GPa).

To the best of our knowledge, most of the investigated parameters are reported for the first time and hoped to stimulate the succeeding studies and offer practical information for the future experiments.

## REFERENCES

[1]  S N Rashkeev, S Limpijumnong and W R L Lambrecht Phys. Rev. B 59 2737 (1999).
[2]  V Shaposhnikov, A Krivosheeva, V Borisenko, J L Lazzari and F d'Avitaya Phys. Rev. B 85 205201 (2012).
[3]  T Ouahrani }O Yasemin tekin c¸iftci and M Mebrouki J. Alloys Compd. 610 372 (2014).
[4]  K T Zawilski, S D Setzler, P G Schunemann and T M Pollak J. Opt. Soc. Am. B 23 2310 (2006).
[5]  S N Rashkeev and W R L Lambrecht Phys. Rev. B 63 165212 (2000).
[6]  Mater. Res. Soc. Bull. 23, No. 7 (1998).
[7]  P. Schunemann, Laser Focus World (April, 1999), p. 85.
[8]  G D Zhang, X T Tao, H P Ruan, S P Wang and Q Shi J. Cryst. Growth 340 197 (2012)
[9]  K. Sato, G.A.Medvedkin T. Ishibashi, T. Nishi, K. Yonemitsu and K. Hirose: Digest 24th Annual Conf. Mgn. Soc. Jpn. Tokyo, Sept. 2000, p. 372 (2000)
[10]  A.S. Verma, S. Sharma, V.K. Jindal, Mod. Phys. Lett. B 24 (2010) 2511.
[11]  A.S. Verma, Phys. Status Solidi B 246 (2009) 192.
[12]  A.S. Verma, D. Sharma, Phys. Scr. 76 (2007) 22.
[13]  I. H. Choi and D. H. Lee, Journal of the Korean Physical Society, Vol. 44, No. 2, February 2004, pp. 403-407.
[14]  G.K.H. Madsen, P. Blaha, K. Schwarz, E. Sjöstedt, L. Nordström, Phys. Rev. B 64 (2001) 195134.
[15]  K. Schwarz, P. Blaha, G.K.H. Madsen, Comput. Phys. Commun. 147 (2002) 71.
[16]  Blaha, P., Schwarz, K., Madsen, G. K. H., Kvasnicka, D., Luitz, J., Laskowsk, R., Tran, F., Marks, L., & Marks, L. (2019). WIEN2k*:* An Augmented Plane Wave Plus Local Orbitals Program for Calculating Crystal Properties*.* Techn. Universitat.
[17]  L W Shi, J Hua, Y Qin, Y P Duan, L Wu, X Q Yang and G Tang J. Alloys Compd. 611 210 (2014).
[18]  H J Monkhorst and J D Pack Phys. Rev. B 13 5188 (1976).
[19]  G Kresse and J Hafner Phys. Rev. B 47 558 (1993).
[20]  G Kresse and J Furthmuller Phys. Rev. B 54 11169 (1996).
[21]  G Kresse and J Furthmuller Comput. Mater. Sci. 6 15 (1996).
[22]  G Kresse and D Joubert Phys. Rev. B 59 1758 (1999).
[23]  J Perdew, K Burke and M Ernzerhof Phys. Rev. Lett. 77 3865 (1996).
[24]  B Saha, T D Sands and U V Waghmare J. Appl. Phys. 109 073720 (2011).
[25]  A Togo Phonopy, http://sourceforge.net/projects/phonopy/

[26]  S C Abrahams and J L Bernstein J. Chem. Phys. 55 796 (1971).

[27]  F. Chiker, B. Abbar, A. Tadjer, H. Aourag, B. Khelifa, Mater. Sci. Eng. B 98 (2003) 81.

[28]  J.L. Shay, J.H. Wernick, Ternary Chalcopyrite Semiconductors: Growth, Electronic Properties and Applications, Pergamon Press, Oxford, 1974.

[29]  F. Birch, "Elasticity and constitution of the Earth's interior," Journal of Geophysical  Research, vol. 57, no. 2, pp. 227–286, 1952.

[30]  R Gautam, P Singh, S Sharma, S Kumari and A S Verma Mater. Sci. Semicond. Process. 40  72 (2015)

[31]  H.J. Hou, H.J. Zhu, S.P. Li, T.J. Li, L. Tian, J.W. Yang, Indian J. Phys. 92 (2018) 315–323.

[32]  V. L. Shaposhnikov, A. V. Krivosheeva, V. E. Borisenko, J.-L. Lazzari, and F. Arnaud d'Avitaya Phys. Rev. B 85, 205201 ( 2012).

[33]  Landolt-Börnstein, in Condensed Matter, Ternary Compounds,Organic Semiconductors, New Series, Group III, edited by O. Madelung, U. Rössler, and M. Schulz, Vol. 41E (Springer-Verlag,Berlin, 2000).

[34]  W. Hoenle and H. G. von Schnering, "Verfeinerung der kristallstriktur von CdGeP 2 ," Zeitschrift fuer Kristallographie, vol. 155, pp. 319–320, 1981.

[35]  M Born and K Huang Dynamical Theory of Crystal Lattices (Oxford: Clarendon) (1954)

[36]  W Voigt Lehrbuchder Kristall physik,Teubner, Leipzig (1928)

[37]  A Reuss and Z Angew. Math. Mech. 8 55 (1929)

[38]  R Hill Proc. Phys. Soc. Lond. A 65 349 (1952)

[39]  J F Nye Physical Properties of Crystals (Oxford: Oxford University Press) (1985)

[40]  A S Verma, S Sharma, R Bhandari, B K Sarkar and V K Jinda Mater. Chem. Phys. 132 416 (2012)

[41]  F W Ohrendofr and H Haeuseler Cryst. Res. Technol. 34 351 (1999)

[42]  C Lee and X Gonze Phys. Rev. B 51 8610 (1995)